GLOBAL-LOCAL ANALYSIS AND OPTIMIZATION OF A COMPOSITE CIVIL TILT-ROTOR WING

Masoud Rais-Rohani, Ph.D., P.E.
Department of Aerospace Engineering
Mississippi State University
Mississippi State, MS 39762

Phone: (601) 325-7294
Fax: (601) 325-7730
E-mail: masoud@ae.msstate.edu

Table of Contents

Abstract

This report gives highlights of an investigation on the design and optimization of a thin composite wing box structure for a civil tilt-rotor aircraft. Two different concepts are considered for the cantilever wing: (a) a thin monolithic skin design, and (b) a thick sandwich skin design. Each concept is examined with three different skin ply patterns based on various combinations of 0, ±45, and 90 degree plies. The global-local technique is used in the analysis and optimization of the six design models. The global analysis is based on a finite element model of the wing-pylon configuration while the local analysis uses a uniformly supported plate representing a wing panel. Design allowables include those on vibration frequencies, panel buckling, and material strength. The design optimization problem is formulated as one of minimizing the structural weight subject to strength, stiffness, and dynamic constraints. Six different loading conditions based on three different flight modes are considered in the design optimization. The results of this investigation reveal that of all the loading conditions the one corresponding to the rolling pull-out in the airplane mode is the most stringent. Also the frequency constraints are found to drive the skin thickness limits, rendering the buckling constraints inactive. The optimum skin ply pattern for the monolithic skin concept is found to be $((0/\pm 45/90/(0/90)_2)_s)_s$ while for the sandwich skin concept the optimal ply pattern is found to be $((0/\pm 45/90)_{2s})_s$.

Introduction

The tilt-rotor aircraft combines the high-speed efficiency of fixed-wing flight with the utility of vertical or short takeoff and landing (V/STOL). There are two wing-tip mounted nacelle-rotor assemblies which can rotate to a vertical position for helicopter-type maneuvers and to a horizontal position for high-speed horizontal flight as depicted in Fig. 1.
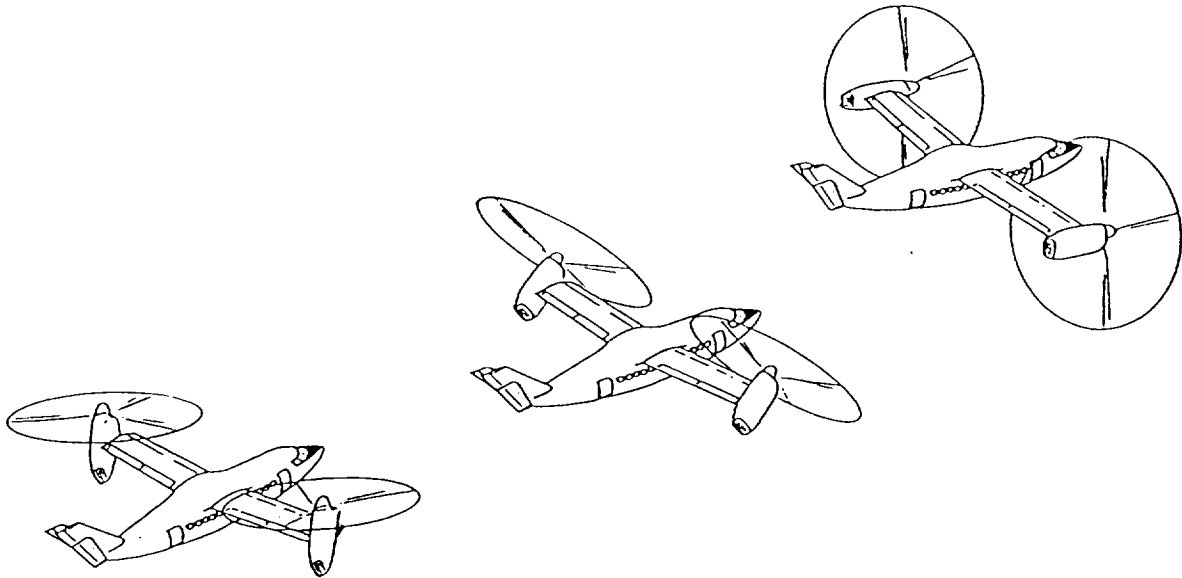

Figure 1. Tilt-rotor aircraft in helicopter, conversion, and airplane modes.

With the success of the Bell XV-15 program and its derivative the Bell-Boeing V-22, more consideration is being given to the tilt-rotor concept for civilian applications with emphasis on high-speed performance and productivity[1]. An aeroservoelastic design analysis to maximize the productivity index, a measure of how fast a given payload can be delivered for a given block of fuel, was carried out by Sterner and Schrage[2]. Although the work was limited to one loading condition (2-g Jump Takeoff), with a plate model for static analysis, its results noted the importance of minimizing the wing-box structural weight for a tilt-rotor aircraft.

In a study by Rogers and Reisdorfer[3] it was shown that in order to meet the high-speed cruise requirements of the Civil Tilt-Rotor (CTR) aircraft, the fuselage must be adequately streamlined, and the wing compressibility drag must be reduced as much as possible. Reducing the wing maximum-thickness-to-chord ratio (t/c) offers a way to reduce the compressibility drag by increasing the drag-divergence Mach number. While a reduction in t/c would be advantageous for aerodynamic efficiency in high-speed cruise, it would normally have an adverse effect on wing stiffness as it reduces the wing cross-sectional moment of inertia in vertical bending. However, it was shown by Popelka et al.[4], in an aeroelastic tailoring study for a composite tilt-rotor wing, that through proper blend ratios of ±45°, 0°, and 90° layers in the wing skin, the wing box could be tailored for a more favorable performance at an acceptable prop-rotor stability margin. Although no formal design optimization was carried out in that study, the results indicated that it is possible to reduce t/c from 23% to 18% with minimal weight penalty over the baseline wing design.

The complexity of the tilt-rotor wing system is manifested in terms of wing-rotor-pylon interactions.[5] The aeroelastic instability or whirl flutter stemming from wing-rotor-pylon coupling is found to be the most critical mode of instability demanding careful consideration in the preliminary wing design.[6-12] The placement of wing fundamental natural frequencies in bending and torsion relative to each other and relative to the rotor 1/rev frequencies is found to have a strong influence on the whirl flutter.[13]

The goal of this research investigation is the design and optimization of a thin composite wing box structure for a civil tilt-rotor aircraft leading to a minimum-weight wing design. With focus on the structural design, the wing aerodynamic shape and the rotor-pylon system are held fixed. The initial design requirement on drag reduction set the airfoil maximum thickness-to-chord ratio (t/c) to 18%. The airfoil section is a scaled down version of the 23%-thick airfoil used for V-22 wing design.

A constrained design optimization problem is formulated and solved to determine the optimum alignment and sizing of composite skin plies as well as sizing of stringers, spars, and ribs to alleviate the loss of structural stiffness due to reduced t/c while simultaneously reducing the wing structural weight. The analysis and optimization studies are based on MSC/NASTRAN finite element code.

A global-local procedure is used in this investigation to arrive at an optimal design. In this procedure the global finite-element model of the wing is optimized first based on specified strength and dynamic constraints. Then the individual skin panels and spar webs are examined for local failure using a panel failure analysis/optimization code. For the

monolithic plate the only mode of failure considered is buckling, whereas for the sandwich plate in addition to buckling the shear crimping, intracell buckling, and wrinkling are also considered.

If the local analysis indicates the panel is safe, then its thickness in the global model is adequate. If the panel fails in the local analysis, it is then optimized locally for minimum weight subject to constraints against material and structural failure. The local optimization is performed based on the loads extracted from the global finite-element model using the ply thickness in the global model as the minimum gage. The optimal thickness obtained from local optimization is then used in the global finite-element model to check for any constraint violation. If any constraint violation is detected in the global model, then the global model is reoptimized with the panel thickness obtained from the local code as minimum gage.

The panel analysis/optimization code analyzes rectangular simply-supported monolithic as well as sandwich plates with composite face sheets. The face sheets are made to be balanced and symmetric about the individual face sheet midplane, thus, eliminating the extension-bending coupling.

Global Wing Box Model

The CTR wing box is untapered, and has a semispan of 291 in., measured from the fuselage centerline to the wing tip. From station 0 (i.e., the fuselage centerline) to station 38, the wing box is unswept and has no dihedral. Outside of station 38, it has a forward sweep of 6° and a dihedral of 2°. The single-cell wing box extends in the chord wise direction from the front spar located at 5% chord to the aft spar located at 55% chord. Throughout this study the external wing geometry is held fixed.

The upper and lower skins are each supported by five stringers. The fore and aft spars have flat shear webs with top and bottom caps. There are twelve ribs supporting the skin and stringers along the span. In this study, the number of ribs is held fixed at ten.

The MSC/NASTRAN finite element model of the wing consists of linear CQUAD4 elements for the skin, spar webs, and ribs and CBAR elements for stringers and spar caps. PCOMP property cards with a MAT8 material card are used to model the plate elements. Each plate element is assumed to have 32 layers. The stringers and spar caps have quasi-isotropic lay-up modeled by PBAR property cards.

The tip rotor-nacelle system is modeled by a group of RBAR elements. These elements generate internal multi-point constraint (MPC) equations. These MPC equations determine the deflection of the nodes defined by the RBAR element as rigid body motion only. Since the design has to be evaluated in each of the three different flight modes, the model contains three separate tip models portraying the nacelle in airplane, conversion, and helicopter modes. The finite element model of the wing-nacelle configuration with the nacelle in conversion mode is shown in Fig. 2.
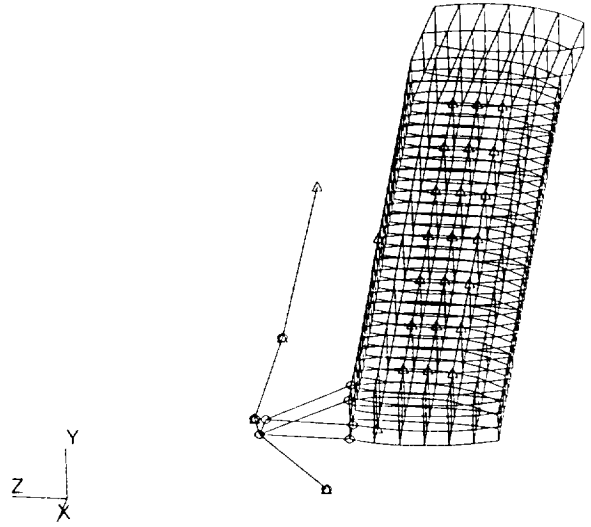
3

Figure 2. Wing-nacelle finite element model

All wing box components are made of graphite-epoxy composite materials. The stiffness and strength allowables used in this study are listed in Table 1.

Table 1. Graphite-epoxy material properties

Strength Properties		Stiffness Properties		Specific Weight	
$X_t=$	150.0e3 psi	$E_1=$	30.0e6 psi	$\rho=$	0.056 lb/in^3
$X_c=$	100.0e3 psi	$E_2=$	0.75e6 psi		
$Y_t=$	6.0e3 psi	$G_{12}=$	0.375e6 psi		
$Y_c=$	17.0e3 psi	$v_{12}=$	0.25		
$S=$	10.0e3 psi				

X_t and X_c represent the allowable strength values of the material along the fibers in tension and compression, respectively. Y_t and Y_c represent the allowable strength values of the material perpendicular to the fibers in tension and compression, respectively. S represents the allowable in-plane shear strength of the material. E_1 and E_2 represent the moduli of elasticity along the fibers and perpendicular to the fibers, respectively. G_{12} represents the in-plane shear modulus of the material, v_{12} is the in-plane Poisson's ratio of the material, and ρ is the specific weight of the material.

As part of this investigation, a detailed mesh refinement process with convergence assessment techniques was performed. MSC/PATRAN is used for the mesh refinement and convergence process. Since it is desired to maintain the same type of elements throughout the mesh, i.e., linear elements, the model is refined using the h-refinement technique. The refined model used for design optimization has 640 CQUAD4 and 448 CBAR elements for a total of 3,480 degrees of freedom.

4

Local Panel Model

The local model describes a rectangular skin or spar web panel of the wing box. A skin panel is defined here as a skin section bounded by two adjacent ribs and two adjacent stringers or a stringer and a spar cap. In this research, two different skin configurations are compared for optimum design. The configurations are: a thin skin, "heavily" stiffened panel and a thick skin, "lightly" stiffened panel. In the first case, the panel is made of a thin monolithic composite laminate, and as such, the stringers and spar caps are theoretically forced to be larger (heavier) in order for the wing box to carry the required bending loads. In the second case, the skin consists of thicker sandwich panels, which can carry more bending loads and, therefore, should allow for smaller (lighter) stringers and spar caps.

The panels are investigated for instability due to in-plane forces N_x, N_y, and N_{xy}, as shown in Figure 3. These loads are calculated in the global analysis and are compared with the corresponding critical values found by the local analysis code. In the local stability analysis, both monolithic and sandwich panels are assumed to be simply supported along all four edges.
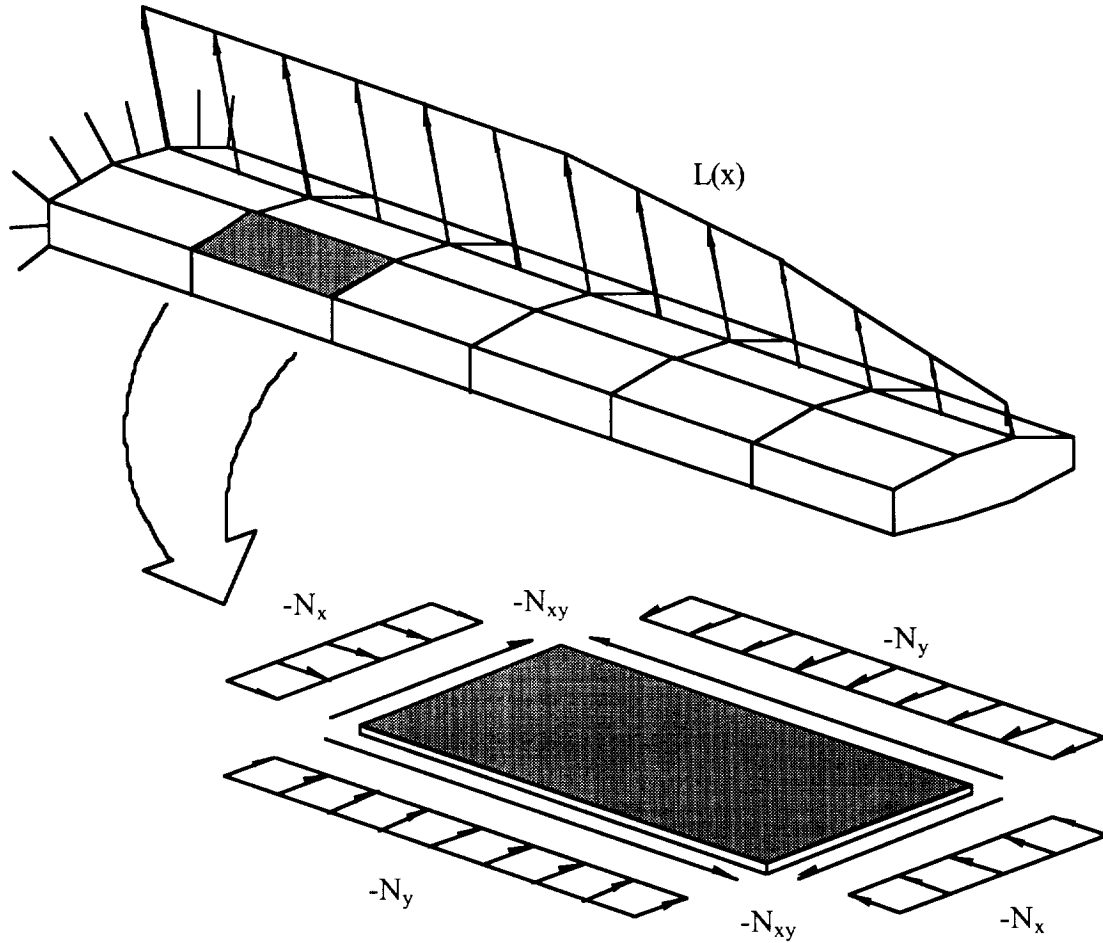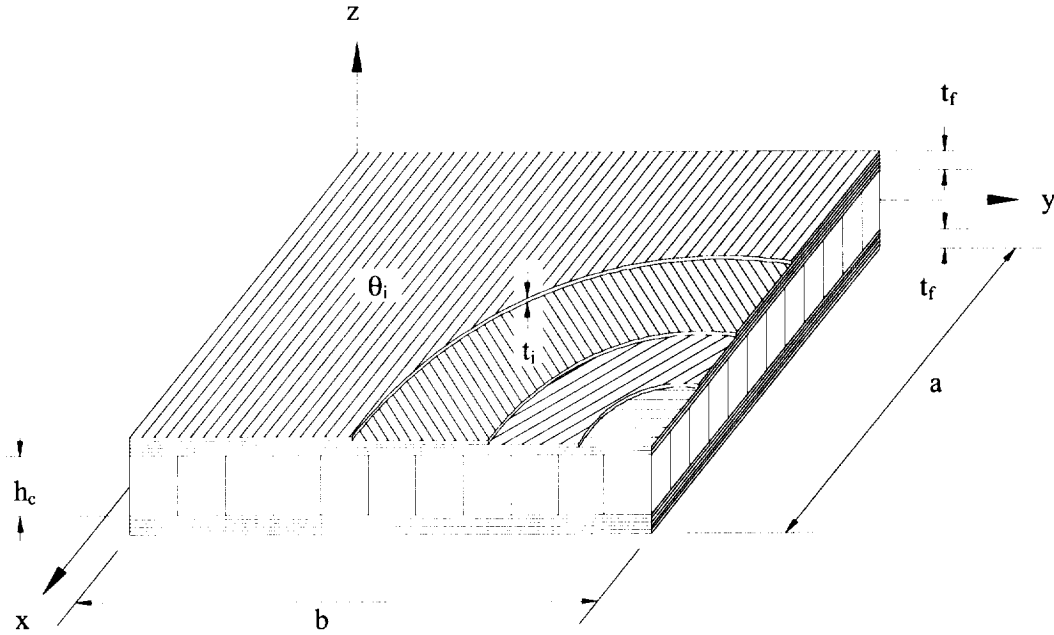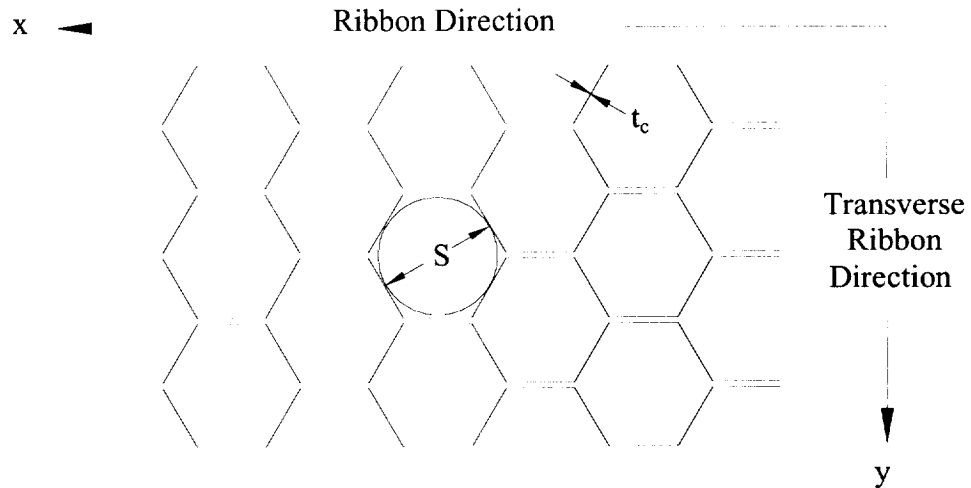

Figure 3. A wing skin panel and associated in-plane loads

5

The geometric and structural parameters of a composite sandwich plate are shown in Figure 4. The parameters consist of the planform dimensions a and b, ply thickness (t_i) and orientation angle (θ_i), face sheet thickness (t_f), core cell size (S), core foil thickness (t_c), and overall core thickness (h_c). Figure 4 (b) depicts the orientation of the honeycomb core. The honeycomb core is strongest and stiffest along the ribbon direction. Since plates of relatively high aspect ratio (i.e., a/b ≈ 5) are analyzed in this study, the core efficiency is maximized by placing the ribbon direction parallel to the longest side.

(a) Sandwich plate with layered face sheets

(b) Honeycomb core in plan view

Figure 4. Components of a honeycomb-core composite sandwich plate

6

The sandwich plates have aluminum honeycomb cores. The stability analysis of a composite sandwich panel is generally more complicated than that of a monolithic panel. In addition to panel buckling, sandwich plates with cellular cores are also susceptible to other modes of instability such as core shear crimping, intracell buckling, and face sheet wrinkling. The mathematical development for each of these failure modes is given by Clements[17] and is not repeated here. Since sandwich plates are not necessarily thin, the effects of transverse shear through the core thickness must be considered in the analysis. However, the transverse shear effects are ignored in the case of a laminated plate as it is assumed to be thin and in a state of plane stress.

Flight Scenarios and Associated Wing Loads

In a study by BHTI[14] eleven different flight scenarios were examined to assess the internal loads in the wing. As was established in the previous study,[15] six of these flight scenarios were considered to be most critical and encompassing of the different flight modes, i.e., airplane mode, conversion mode, and helicopter mode. The wing loads for each scenario correspond to the most critical point along each maneuver envelope. The known resultant forces are broken into distributed loads along the span of the wing box for use in the finite-element analysis. In this research, the lift force is modeled by a chord wise and a spanwise distribution. The spanwise distribution is quasi-elliptical and since the quarter-chord of the wing is approximately located at the center of the wing box, the chord wise distribution is modeled triangularly, with the vertex at the center of the wing box. This model allowed for a somewhat realistic representation of the lift on the wing and helped to alleviate stress concentration points in the structure. In each case, the lift load intensity is chosen such that it produces the same wing root moment as the corresponding resultant force.

In this study, the loads associated with each flight scenario are treated as a set of static loads without considering any aeroelastic load redistribution. The six flight scenarios considered in this research are given in Table 2:

Table 2. Flight modes and associated conditions

Flight Mode	Condition
Helicopter	1. 2.0g jump takeoff
	2. 50 ft/s gust @ 80 knots
Conversion	3. 110 knot symmetrical pull-up with 75° nacelle incidence
	4. 185 knot 3.0g symmetrical pull-up with 0° nacelle incidence[a]
Airplane	5. 289 knot 4.0g symmetrical pull-up
	6. 390 knot 3.2g left rolling pull-out

[a] The fourth flight scenario shows a nacelle incidence of approximately 0°. While this fact is not specifically mentioned in Ref. [14], the rotor forces and center of gravity locations indicate a nacelle orientation of 0°. Therefore, flight scenario number four is considered as a loading subcase for the airplane rather than the conversion mode in the finite-element analysis.

Aeroelastic and Dynamic Requirements

The tilt-rotor wing box must be designed to not only meet the strength, but also the stiffness requirements that are unique to the tilt-rotor configuration. In the design used in this study, the rotor assembly attached to the tip of the wing box weighs over 1500 pounds. Each rotor blade, also known as a prop-rotor, has a radius of over 236 inches and can rotate up to approximately 380 RPM, thus, resulting in extremely large dynamic and aerodynamic loads on the wing. When these loads are coupled with the flexibility of the wing box structure, they can lead to severe dynamic and aeroelastic instabilities.

The aeroelastic instabilities associated with the tilt-rotor configuration are the result of the combination of three types of forces: 1) aerodynamic forces acting on the rotor, nacelle, and the wing as a result of airflow, 2) inertial forces resulting from mass acceleration of the rotor and wing, and 3) elastic forces due to deflections of flexible rotors, nacelle, and the wing. Two types of instabilities have to be considered in the design of a tilt-rotor wing box: aeromechanical instability and aeroelastic instability.

Aeromechanical instability, or simply mechanical instability, takes the form of what is commonly referred to as "ground resonance" or "air resonance" depending on where it takes place.[6] This instability occurs when the position of one rotor blade shifts with respect to the other in the plane of rotation causing a relative shift of the rotor center of gravity. The onset of whirling results from the relative shift of the rotor c. g. from the axis of rotation and causes the rotor hub to vibrate. This vibration in turn causes further offset of the rotor center of gravity and therefore more vibration. The inevitable divergence can quickly destroy the rotor system. This instability can be avoided by stiffening the rotor blades so that their in-plane natural frequencies are greater than the rotor speed.[6] Since this instability can be avoided through careful design of the rotor system, it is not a considered in this study.

The most critical aeroelastic instability of the tilt-rotor aircraft is a type of flutter that is seen in forward flight when the prop-rotors are acting as propellers. The tilt-rotor aircraft exhibits a phenomenon known as *whirl flutter*. The onset of whirl flutter is caused when the flapping motion of the rotor blades and the associated forces combine with wing flexibility to cause the prop-rotor axis of rotation to be perturbed from its intended direction. As the prop-rotor turns, the mast will whirl about its intended axis of rotation, hence the name whirl flutter. At relatively low speeds, this oscillation will damp itself out, but at a speed higher than some critical value, this oscillation becomes unstable. The onset of whirl flutter is mainly influenced by the wing natural frequencies of vibration in bending and torsion and the in-plane bending natural frequencies of the rotor blades, and can be avoided by proper placement of wing natural frequencies.

Through an extensive study, BHTI[14] has established a wing frequency placement guide for the preliminary designs of tilt-rotor wing box structures. This guide consists of the following constraints:

1. The first vertical bending frequency of the wing (ω_v) must be less than 80% of its first horizontal bending frequency (ω_h).

2. The first horizontal bending frequency (ω_h) must be approximately 85% of the 1/rev of the prop-rotor in airplane mode.

3. The first torsional frequency of the wing (ω_t) must be at least 115% of the 1/rev of the prop-rotor in helicopter mode.

The helicopter term 1/rev generally refers to the lowest blade vibration caused by the presence of an object in the vicinity of the blade path. For the tilt-rotor design, the 1/rev in airplane mode is 4.8 Hz, and the 1/rev in helicopter mode is 6.3 Hz. This frequency placement guide is used throughout this study to form constraints on dynamic and aeroelastic instabilities of the wing box.

Design Sensitivity Analysis

A detailed sensitivity analysis was performed in order to assess the influence of certain structural parameters on the frequency response of the wing box. The structural parameters considered were simplified for this work. The upper and lower skins were assumed to have uniform properties with three discrete ply patterns defined as: $(0/90/\pm45)_{2s}$, $((0/90)_3/\pm45)_s$, and $((\pm45)_3/0/90)_s$. The spar webs were considered to be uniform as well. In addition, all four spar caps were considered as a single entity. All ten stringers, five on the upper surface and the five on the lower surface, were also considered as a single entity. The four structural parameters considered in the sensitivity analysis are summarized in Table 3. The details of the sensitivity analysis can be found in Ref. 16.

Table 3. Structural parameters considered in the design sensitivity study

Parameter	Description	Range of Values
t_{sk}	Total skin thickness	0.1 to 0.6 in
A_{st}	Total stringer cross-sectional area	0.1 to 2.5 in^2
A_{sc}	Total spar cap cross-sectional area	0.1 to 2.5 in^2
t_{sw}	Total spar web thickness	0.1 to 0.6 in

As part of preprocessing, a composite laminate analysis program was used to determine effective laminate engineering properties (i.e., $\bar{E}_x, \bar{E}_y, \bar{G}_{xy},$ and $\bar{\nu}_x$) for input into MSC/NASTRAN finite element code to calculate the wing box natural frequencies. These effective engineering constants depend on the orientation, thickness, and engineering properties of the individual plies in the laminate, and are determined based on classical lamination theory.

First a modal analysis was performed to see how the first vertical bending, first horizontal bending and first torsion natural frequencies of the wing were influenced by each of the structural parameters described in Table 3. This analysis was performed for both airplane and helicopter configurations.

The results of the modal analysis, described in detail in Ref. [16], show that in both airplane and helicopter configurations the stringers have the most influence on the first vertical

bending frequency, followed very closely by the skin thickness. The spar caps have minor influence on this modal frequency, and the spar webs have almost no influence. The skin, spar caps, and stringers are found to have a major influence on the horizontal bending frequency in the order mentioned. The spar web is found to have almost no influence on this mode of vibration in both helicopter and airplane configurations. The skin is also found to have a major effect on the torsion frequency. Stringers and spar caps are found to have some influence on this mode in the helicopter configuration, but almost no impact when the nacelle is in horizontal (i.e., airplane) position. The spar webs are also found to have very minor effect on this mode of vibration in both configurations.

The sensitivity derivatives of the natural frequencies with respect to skin thickness, spar-cap and stringer cross-sectional areas, and spar-web thickness were determined for each of the three skin ply patterns described in Table 3.

MSC/NASTRAN does have a sensitivity analysis capability as part of its optimization solution sequence. However, it requires the behavioral characteristics for the sensitivity derivatives sought to be formulated as design constraints, and even then it only provides the derivatives of active constraints. As a result of this limitation, the sensitivity derivatives of the natural frequencies with respect to each parameter are determined outside of the finite-element solution sequence as part of the post-processing. The forward finite-difference method was used to evaluate these derivatives. A stepsize analysis was first conducted to determine an acceptable stepsize to assure derivative accuracy, then a modal analysis was conducted for a perturbed value of each parameter. Each finite-difference sensitivity coefficient was calculated as:

$$\frac{\partial \omega_j}{\partial p_i} = \frac{\omega_j(p_i + \Delta p_i) - \omega_j(p_i)}{\Delta p_i} \tag{1}$$

where ω_j (j=1, 2, 3) represents the jth natural frequency, p_i (i=1, 2, 3, 4) represents the ith parameter, and Δp_i represents the ith parameter stepsize.

To determine the effect of spar-cap cross-sectional area on the derivatives of the natural frequencies with respect to skin thickness, the values of stringer cross-sectional area and spar web thickness were held at their average values while Eq. (1) was used repeatedly for different values of spar-cap cross-sectional area between its upper and lower bounds. This approach was repeated for stringer cross-sectional area and spar web thickness as well. A similar procedure was performed for the derivatives of natural frequencies with respect to the other three parameter as well.

The results of the sensitivity analysis primarily demonstrated the effect of values of the other parameters on the sensitivity coefficients of the parameter at hand. In other words, the direction of search in the optimization process depends on the initial design and associated derivatives of the objective function and constraints with respect to the selected design variables. The modal and sensitivity analysis help us draw the following conclusions:

1. The skin ply pattern has the greatest influence on the vibration characteristics of the structure.
2. An increase in wing skin thickness causes the greatest separation between the first vertical bending and first torsion natural frequencies of the structure.
3. The quasi-isotropic skin laminate generally yields average values for the natural frequencies and their sensitivity derivatives in both airplane and helicopter configurations.
4. The magnitudes of the sensitivity derivatives of the primary natural frequencies with respect to each parameter are influenced to varying degrees by the values of the other parameters.

Design Optimization Problem

The wing design optimization problem is formulated in the form of a standard constrained optimization problem. The optimum set of design variables X is sought to

$$
\begin{aligned}
&\text{Min.} \quad W(X) \\
&\text{S.T.} \quad g_s(X) \geq 0 \\
&\qquad\quad g_d(X) \geq 0 \\
&\qquad\quad X^l \leq X \leq X^u
\end{aligned}
\qquad (2)
$$

where W is the wing-box structural weight. The structural and dynamic/aeroelastic requirements are represented by the inequality constraints g_s and g_d, respectively. The lower and upper bounds on each of the design variables is denoted by x^l and x^u, respectively.

The structural constraints are formulated in terms of strength allowables. For one-dimensional members (i.e., stringers and spar caps), they are expressed according to the maximum-stress failure criterion and material stress allowables, whereas for two-dimensional members (i.e., skin and web) they are expressed based on the maximum-strain failure criterion and material strain allowables. The brittle failure of graphite-epoxy panels is predicted more accurately with the maximum-strain failure criterion than most other commonly used failure criteria.

The dynamic/aeroelastic constraints are formulated in terms of wing fundamental bending and torsion frequencies and the frequencies of the rotor system. The frequency placement guide mentioned earlier is used in the formulation of frequency constraints.

The modal analysis has shown that the first vertical bending, the first horizontal bending, and the first torsional modes correspond to the first, second, and third normal modes, respectively. While for each of the first and third conditions stated in the placement guide a single inequality constraint is used, for the second condition two inequality constraints are used — one to impose a lower bound and another to impose an upper bound on ω_h. A 5% margin is used in each case.

11

It is important to point that the selection of the weight as the objective function is rooted in improving the performance of the aircraft, and no link is made between the weight and the manufacturing cost of the wing structure.

Description of Design Variables

Each of the upper and lower surfaces is divided into 18 segments, yielding a total of 36 segments. Each bay of the wing box, which refers to an enclosed volume between two adjacent ribs, contains two segments in the upper surface, two segments in the lower surface, one for the fore spar, and one for the aft spar. The third stringer (i.e., one centrally located in the chord wise direction) represents the dividing line between the forward and aft regions of the skin in each bay. There are a total of 36 design segments in the upper and lower wing skins. Allowing the skin to vary in the chord wise as well as in the spanwise directions allows for greater tailoring of the wing skin in the optimization process. In addition, each skin panel is assumed to have 32 plies of equal thickness. Through the use of the DLINK card in MSC/NASTRAN, the overall skin thickness is set up as the only independent design variable in each segment. Figure 5 contains a visual representation of how the design segments/variables are distributed throughout the wing box.

In order to investigate the effect of ply pattern on the wing design, three discrete ply patterns are chosen to vary externally to MSC/NASTRAN. The ply patterns studied are: $((0/\pm45/90)_{2s})_s$, $((0/\pm45/90/(0/90)_2)_s)_s$, and $((0/(\pm45)_3/90)_s)_s$. The first ply pattern is a quasi-isotropic laminate and its ply percentages are (25%/50%/25%), where there are 25% 0's, 50% ±45's, and 25% 90's. The second ply pattern is one that exhibits a significantly greater bending stiffness and its ply percentages are (37.5%/25%/37.5%). The third ply pattern exhibits greater shear stiffness and its ply percentages are (12.5%/75%/12.5%).

In the case of sandwich skin the honeycomb core material is modeled as an orthotropic layer using the PCOMP property card, with its own separate DESVAR or design variable card. The properties of the honeycomb core used in the global finite-element model appear in Table 4. These properties refer to an aluminum honeycomb core material with a cell diameter of 0.25 inches and a foil thickness of 0.002 inches.
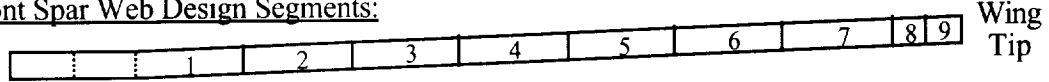
Table 4. Aluminum honeycomb-core material properties

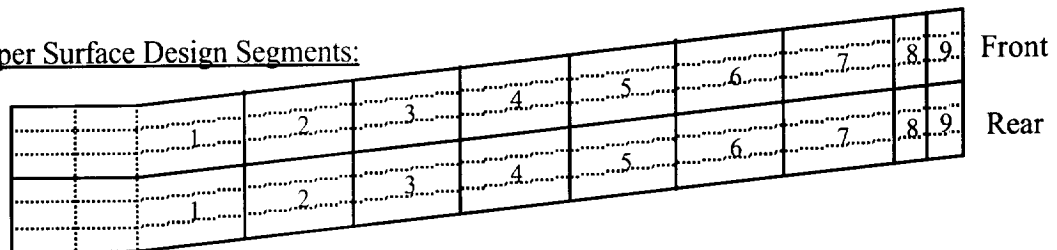| Strength Properties		Stiffness Properties		Specific Weight
$X_t=$	500.0 psi	$E_x=$	140.0e3 psi	$\rho=$ 0.0025 lb/in^3
$X_c=$	500.0 psi	$E_y=$	70.0e3 psi	
$Y_t=$	200.0 psi	$G_{xy}=$	55.0e3 psi	
$Y_c=$	200.0 psi	$G_{xz}=$	66.0e3 psi	
$S=$	250.0 psi	$G_{yz}=$	29.8e3 psi	
		$\nu_{xy}=$	0.30	

The cross-sectional areas of stringers and spar caps are assumed to be constant along the wing span. Therefore, each stringer / spar cap is represented by a single DESVAR or design variable card in MSC/NASTRAN. Since the moment of inertia of each stiffener about its

own centroidal axis is small compared to the corresponding parallel axis term, the stiffeners are simply modeled by their cross-sectional areas.
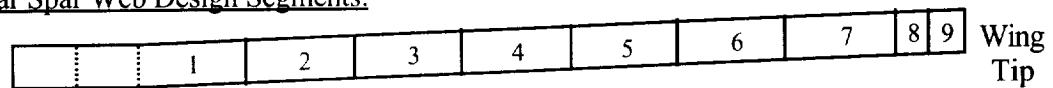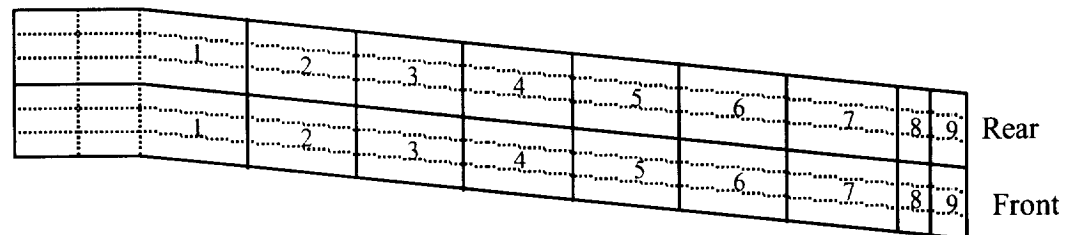
Front Spar Web Design Segments:

Upper Surface Design Segments:

Rear Spar Web Design Segments:

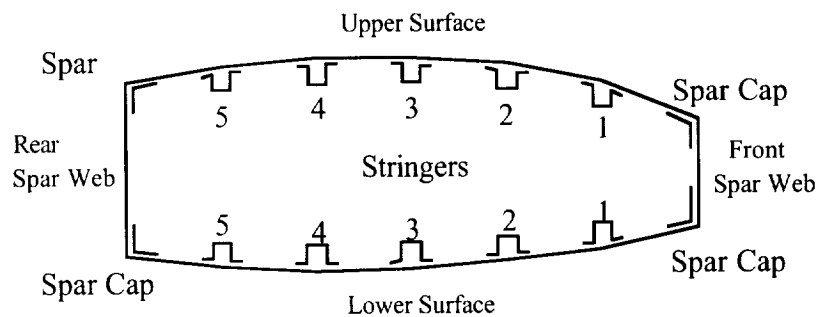Lower Surface Design Segments:

Wing Cross-Section:

Figure 5. Description of wing design variables

Each spar web is divided into nine segments (see Fig. 5) with one thickness design variable per segment. Each segment is modeled as a laminate with four layers, all having a $(\pm 45)_s$ lay-up. Each rib in the swept region of the wing is given its own design variable consisting of the same $(\pm 45)_s$ lay-up. The ribs in the straight region of the wing including the one at the fuselage centerline are assumed to have the same properties as the rib located at break point.

The side constraints, or minimum gage constraints on the design variables are:

$$0.005 \le t_{ply} \le 0.1 \text{ in}$$
$$0.1 \le t_{core} \le 1.0 \text{ in} \tag{3}$$
$$0.1 \le A_{stiffener} \le 5.0 \text{ in}^2$$

where t_{ply} is the thickness of a graphite-epoxy ply, t_{core} is the thickness of the aluminum honeycomb core, and $A_{stiffener}$ represents the cross-sectional areas of either the stringers or spar caps.

Therefore, there are 78 independent and 400 dependent design variables for the wing concept having a monolithic skin and 114 independent and 400 dependent design variables for the wing with sandwich skin.

Equation 2 is solved using the solution 200 of MSC/NASTRAN based on the modified method of feasible direction.

Summary of Results

A global-local procedure is used in the design optimization of the composite tilt-rotor wing box structure for each of the six different loading conditions described in Table 2. Monolithic wing skin designs are compared to honeycomb-core sandwich skin designs for each of the three discrete skin ply patterns. From this point forward, these design subcases will be referred to in the manner described in Table 5.

Table 5. Description of different skin ply patterns

Subcase	Ply Pattern	Skin Type
1	$((0/\pm 45/90)_{2s})_s$	Monolithic
2	$((0/\pm 45/90/(0/90)_2)_s)_s$	Monolithic
3	$((0/(\pm 45)_3/90)_s)_s$	Monolithic
4	$((0/\pm 45/90)_{2s})_s$	Sandwich
5	$((0/\pm 45/90/(0/90)_2)_s)_s$	Sandwich
6	$((0/(\pm 45)_3/90)_s)_s$	Sandwich

The constraints imposed on the global model include those on the wing box natural frequencies and material strength. The local failure constraints on each panel are imposed through the procedure described earlier in the introduction section.

The initial wing design with monolithic skin (subcases 1 to 3) weighs 1,088 lbs. The initial design for each subcase is based on all design variables being at their respective average values. For subcase 1, the optimization process took seven iterations and 2 hours on an SGI workstation to converge to a design weighing 925 lb. Subcase 2 took thirty six iterations in approximately eleven hours to reach a final weight of 646 lb. Subcase 3 took eight iterations in almost three hours to converge to its final weight of 953 lb.

The initial wing design with sandwich skin (subcases 4 to 6) weighs 1,120 lbs. Subcase 4 took twenty two iterations in almost eleven hours to converge to a final design weighing 692 lb. Subcase 5 took thirteen iterations in four and half hours to reach a final weight of 836 lb. Finally, subcase 6 took four iterations in almost two and a half hours to converge a weight of 1,023 lb.

As was discovered in an earlier research,[15] the loads associated with airplane mode are found to be the most critical. With regard to the vibrational characteristics of the wing, the nacelle orientation is shown to have a minor influence on the bending modes, but a major effect on the torsion mode. This difference is due to the fact that the wing elastic axis does not coincide with the axis of the conversion spindle about which the nacelle rotates from one flight mode to another. As it was also shown in the earlier research, if the wing box satisfied the torsion frequency constraint in the airplane mode, it would also satisfy the same constraint in the helicopter and conversion modes. In other words, the airplane mode is found to be the most critical for torsional vibration.

The final design obtained by optimizing the global finite element model in each subcase is then checked for local failure. Of the six loading conditions used in the global model the most critical one, yielding the largest strain energy in a given panel, is used to extract the panel loads to compare with the critical values found from the local analysis. Strain energy is a response that MSC/NASTRAN can provide, therefore, a computer program was written to manipulate and sort the MSC/NASTRAN output file. The program chooses a load case that corresponds to the maximum strain energy in a given panel and extracts the corresponding in-plane loads.

The local failure analysis of the final design for subcase 1 indicated that the skin and shear web panels are not susceptible to buckling failure. For this design, the stiffness required to satisfy the dynamic constraints seemed to be the only driving factor. The stiffeners in this subcase are found to be heavier than the skin. Also, the weight of the spar webs and ribs are almost negligible compared to that of the skin and stiffeners. This finding is consistent with the result of sensitivity analysis showing that the skin and stiffeners have the largest impact on the dynamic response of the wing box.

The local failure analysis for subcase 2 indicated that the skin and shear web panels would not buckle under the specified edge loads. For this design subcase, the wing skin appears to

be the only major contributor to the weight of the wing box. Also, this design subcase is the lightest among the models with monolithic skins.

For subcase 3 the skin and shear web panels were also found to be safe against buckling, even though the margins of safety against buckling for several panels are less than the corresponding ones in the previous two subcases. For this design subcase, the stiffeners are the major contributors to the weight, but not to the same degree as the skin was in the previous subcase. In this design subcase the skin exhibits very high shear stiffness but low bending stiffness. Therefore, the stiffeners carry most of the bending loads. The objective history for the first three subcases is shown in Fig. 6.
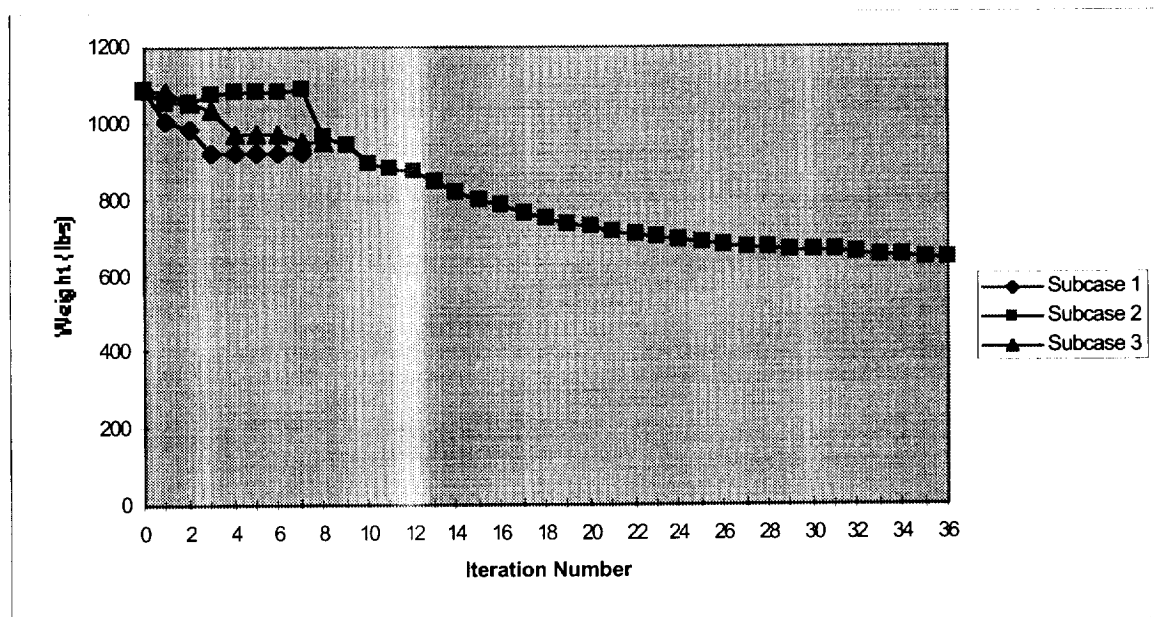

Figure 6. Objective function history for monolithic skin wing models

In the next three subcases, sandwich skin panels are checked for buckling as well as shear crimping, intracell buckling, and wrinkling failure. The skin panels in subcase 4 appear to be safe against any of the local failure modes although the margins of safety against buckling are lower than those in subcase 1. The skin is the major contributor to the weight of the entire structure. For this case, the notion of thick-skin, lightly stiffened structure holds true as the thick skin yielded lighter stiffeners than its counterpart in design subcase 1.

In design subcase 5, the intracell buckling and face sheet wrinkling margins of safety are close to 100%. The buckling and shear crimping margins of safety are also very high. Once again, the ribs and spar webs are negligible contributors to the weight of the optimum wing box. Here also the skin weighed more than the stiffeners.

In design subcase 6, no local failure was observed in skin or shear web panels. Because of the low bending stiffness of the face sheets in the skin panels, the stiffeners become larger. For this reason, the skin is lighter than the stiffeners in this subcase. This design is the

16

lightest among the models utilizing sandwich skins. The objective function history for the last three subcases is shown in Fig. 7.
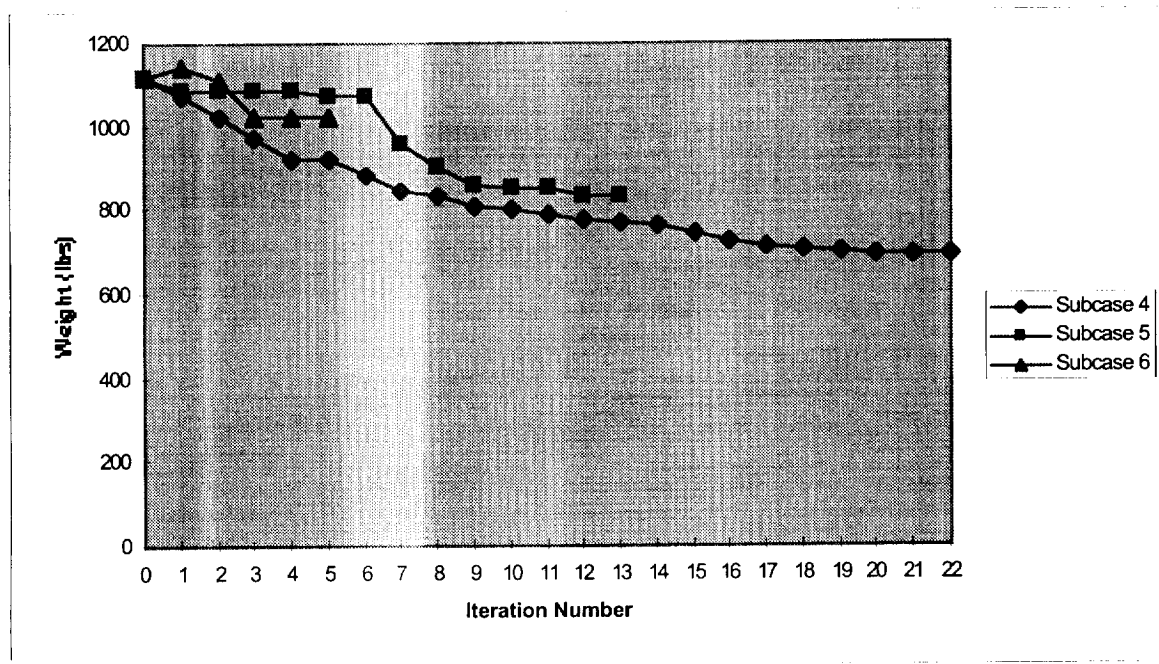

Figure 7. Objective function history for sandwich skin wing models

Generally speaking, the local panel failure constraints were inactive. The side constraints on spar web thickness were less stringent, therefore, those panels were allowed to get thinner and be more critical than the wing skins. Also, it was shown in the design sensitivity study that the spar webs did not contribute much to the dynamic aspects of the wing box. The dynamic constraints on the global model masked the local failure constraints on individual panels.

The optimal weight distribution of individual wing components in design subcases 1 through 6 are given in Table 6. Note that the difference between the total weight in Figs. 6 and 7 and that in Table 6 is because of the inboard wing section that is not changed in the design optimization process.

Table 6. Weight distribution of optimized wing components, lb

Design Subcase	Upper skin	Lower skin	Top stringers	Bottom stringers	Top spar caps	Bottom spar caps	Front spar web	Rear spar web	Ribs	Total
1	174.8	112.3	182.4	162.8	52.1	49.8	12.1	20.3	14.1	781
2	235.7	194.5	23.1	9.0	2.9	3.0	18.3	27.4	13.3	527
3	180.5	108.7	197.3	158.8	53.8	48.8	9.3	15.4	9.4	782
4	202.1	184.6	58.3	34.1	13.1	14.7	10.2	14.1	8.4	540
5	213.7	189.8	96.2	94.5	22.1	30.3	18.8	25.8	11.9	703
6	181.0	147.8	210.3	175.3	50.6	47.7	8.2	15.4	8.7	845

The comparison of monolithic skin design subcases with the corresponding sandwich skin subcases indicates the likelihood of premature entrapment of sandwich skin design subcases in local optimal points. This is evident when comparing the weight distribution in design subcase 2 to that of 5. Although the sandwich skin is lighter in subcase 5 than the monolithic skin of similar ply pattern in subcase 2, the stringers in subcase 5 are four to ten and a half times larger than those in 2. The only way to avoid such entrapment in local optimal points is to use global optimization methods, which are currently not available in MSC/NASTRAN.

As is, the design with the lowest overall weight corresponds to subcase 2 followed by subcase 4 with sandwich skin. It is also interesting to note the effect of ply pattern on the optimal weight. Clearly the wing skin with larger percentage of ± 45° plies results in heavier weight as compared to those with larger percentage of 0° plies.

For additional details about the analysis and results of this investigation refer to Ref. [17].

References

1. Lawrence, D., Reber, R., Hooper, E., Peisen, D. and Leverton, J.W., 1992, "The Civil Rotorcraft Initiative—An Action Agenda," *VERTIFLITE*, Vol. 38, pp. 8-12.
2. Sterner, M. and Schrage, D., "An Approach to Tiltrotor Wing Aeroelastic Optimization Through Increased Productivity," proceedings of the Fourth AIAA/USAF/NASA/OAI Symposium on Multi-disciplinary Analysis and Optimization, Cleveland, OH, September 21-23, 1992, Part 2, pp. 749-759.
3. Rogers, C. and Reisdorfer, D., "Civil Tiltrotor Transport Point Design-Model 940A," NASA-CR-191446, 1992.
4. Popelka, D., Lindsay, D., Parham, T., Berry, V., and Baker, D.J., "Results of an Aeroelastic Tailoring Study for a Composite Tiltrotor Wing," Presented at the 51st Annual Forum of the American Helicopter Society, Fort Worth, TX, 1995.
5. Loewy, R.G., "Aeroelasticity and the Tilt-rotor VTOL Aircraft," VERTIFLITE, Vol. 38, No. 3, 1992.
6. Few, D.D. and Edenborough, H.K., "Tilt-Proprotor Perspective," Astronautics and Aeronautics, December 1977, pp. 28-31.
7. Kvaternik, R.G., "Experimental and Analytical Studies in Tilt-Rotor Aeroelasticity," presented at the AHS/NASA Ames Specialists' Meeting on Rotorcraft Dynamics, February 13-15, 1974.
8. Kvaternik, R.G. and Kohn, J.S., "An Experimental and Analytical Investigation of Proprotor Whirl Flutter," NASA TP-1047, 1977.
9. Reed, W.H.,III, "Propeller-Rotor Whirl Flutter: A State-Of-The-Art Review," Journal of Sound Vibration, Vol. 4, No. 3, 1966.
10. Edenborough, H.K., "Investigation of Tilt-Rotor VTOL Aircraft Rotor-Pylon Stability," Journal of Aircraft, Vol. 5, No. 6, 1968.
11. Alexander, H.R., Hengen, L.M. and Weiber, J.A., "Aeroelastic-Stability Characteristics of a V/STOL Tilt-Rotor Aircraft With Hingeless Blades: Correlation of Analysis and Test," presented at the AHS 30th Annual National Forum, Washington, D.C., May 1974.

12. Vorwald, J.G. and Chopra, I., "Stabilizing Pylon Whirl Flutter on a Tilt-Rotor Aircraft," presented at 32nd AIAA/ASME/ASCE/AHS/ASC Structures, Structural Dynamics, and Materials Conference, Baltimore, MD, April 8-10, 1991.

13. Nixon, M.W., "Parametric Studies for Tilt-rotor Aeroelastic Stability in High-Speed Flight," proceedings of the 33rd AIAA/ASME/ASCE/AHS/ ASC Structures, Structural Dynamics and Materials Conference, Dallas, Texas, April 13-15, 1992, Part 4, pp. 2027-2037.

14. Rogers, C. and Reisdorfer, D., "Civil Tiltrotor Transport Point Design-Model 940A," NASA-CR-191446, 1992.

15. Brunson, S.L., "Design of a Wing Box Structure for the Civil Tilt-Rotor Transport Aircraft," An M.S. Thesis, Department of Aerospace Engineering, Mississippi State University, August 1995.

16. Clements, T.M. and Rais-Rohani, M., "Sensitivity Analysis of a Tilt-Rotor Composite Wing Natural Frequencies with Respect to Structural Parameters," Proceedings of the Eighteenth Southeastern Conference on Theoretical and Applied Mechanics, Tuscaloosa, AL, April 14-16, 1996.

17. Clements, T.M., "Global-Local Analysis and Design Optimization of a Composite Tilt-Rotor Wing Box Structure," An M.S. Thesis, Department of Aerospace Engineering, Mississippi State University, May 1997.